

1-15-2009

# Thermal conductivity of (Zr,W)N/ScN metal/ semiconductor multilayers and superlattices

Vijay Rawat

*Purdue University - Main Campus, vijay.rawat@gmail.com*

Yee Kan Koh

*University of Illinois at Urbana-Champaign*

David G. Cahill

*University of Illinois at Urbana-Champaign*

Timothy D. Sands

*Birck Nanotechnology Center, Purdue University, tsands@purdue.edu*

Follow this and additional works at: <http://docs.lib.purdue.edu/nanopub>



Part of the [Nanoscience and Nanotechnology Commons](#)

Rawat, Vijay; Koh, Yee Kan; Cahill, David G.; and Sands, Timothy D., "Thermal conductivity of (Zr,W)N/ScN metal/semiconductor multilayers and superlattices" (2009). *Birck and NCN Publications*. Paper 368.  
<http://docs.lib.purdue.edu/nanopub/368>

This document has been made available through Purdue e-Pubs, a service of the Purdue University Libraries. Please contact [epubs@purdue.edu](mailto:epubs@purdue.edu) for additional information.

# Thermal conductivity of (Zr,W)N/ScN metal/semiconductor multilayers and superlattices

Vijay Rawat,<sup>1,a)</sup> Yee Kan Koh,<sup>2,b)</sup> David G. Cahill,<sup>2,c)</sup> and Timothy D. Sands<sup>1,d)</sup>

<sup>1</sup>*School of Materials Engineering, School of Electrical and Computer Engineering and Birck Nanotechnology Center, Purdue University, West Lafayette, Indiana 47906, USA*

<sup>2</sup>*Department of Materials Science and Engineering and Materials Research Laboratory, University of Illinois, Urbana-Champaign, Illinois 61801, USA*

(Received 3 October 2008; accepted 22 November 2008; published online 28 January 2009)

The cross-plane thermal conductivities of metal/semiconductor multilayers and epitaxial superlattices have been measured as a function of period by time-domain thermoreflectance at room temperature. (001)-oriented ZrN (metal)/ScN (semiconductor) multilayers and (Zr,W)N/ScN epitaxial superlattices with the rocksalt crystal structure were grown on (001)MgO substrates by reactive magnetron sputtering. A distinct minimum in thermal conductivity at a period of  $\sim 6$  nm is observed for ZrN/ScN multilayers. The minimum thermal conductivity of 5.25 W/m K is a factor of  $\sim 2.7$  smaller than the mean of the thermal conductivities (including only the lattice contributions) of the values measured for films of the constituent materials, and approximately equal to the lattice component of the thermal conductivity of a  $\text{Zr}_{0.65}\text{Sc}_{0.35}\text{N}$  alloy film ( $\sim 5$  W/m K). Alloying the ZrN layers with  $\text{WN}_x$  reduces the lattice mismatch, yielding epitaxial (Zr,W)N/ScN superlattices. The addition of  $\text{WN}_x$  also reduces the thermal conductivity to  $\sim 2$  W/m K, a value that is sufficiently low to suggest promise for these materials as solid-state thermionic generators.

© 2009 American Institute of Physics. [DOI: 10.1063/1.3065092]

## I. INTRODUCTION

Theory and modeling of metal/semiconductor multilayers with optimized Schottky barrier heights and layer thicknesses suggest that these artificially structured materials may be promising for direct thermal-to-electrical energy conversion.<sup>1,2</sup> These solid-state thermionic devices have the potential to deliver higher thermoelectric figures of merit than bulk thermoelectric materials due to energy filtering of the charge carriers and the high electron concentration in the metal, the combination of which is expected to lead to an enhancement in the power factor, which is the product of the electrical conductivity  $\sigma$  and the square of the Seebeck coefficient  $S$ .<sup>3,4</sup> Just as with conventional thermoelectric materials, the cross-plane thermal conductivity should be as small as possible in order to maintain an appreciable temperature difference across the element.

Thermal transport in multilayers has been the subject of several previous studies, and different mechanisms, such as enhanced phonon scattering due to acoustic impedance mismatch,<sup>5–8</sup> alloy scattering,<sup>5,7</sup> phonon scattering due to the presence of defects that accommodate lattice mismatch at the multilayer interfaces,<sup>7</sup> phonon minigap formation<sup>8</sup> and phonon tunneling,<sup>9</sup> have been proposed to explain the thermal transport behavior. In the present study, the first measurements of cross-plane thermal conductivity in epitaxial metal/semiconductor superlattices are presented. The fact that the dominant carriers of thermal energy in bulk semiconductors are phonons, whereas electrons carry the majority of the ther-

mal energy in bulk metals, requires energy transfer between the phonons and the electrons at the metal/semiconductor interface, unlike previously analyzed semiconductor/semiconductor superlattices.<sup>10</sup>

In a previous study,<sup>11</sup> nitride metal/semiconductor multilayers and superlattices were identified as candidate materials for solid-state thermionic generators that operate at elevated temperatures (up to  $\sim 1000$  °C). Rocksalt nitrides offer the potential for lattice matching, tunable barrier heights in the range required for power factor optimization ( $\sim 4-5k_B T$ ),<sup>12</sup> metastable superlattices with nanoscale periods, and high carrier concentrations ( $>10^{21}$  cm<sup>-3</sup>) in the metallic phase. To exploit the potential enhancement in the power factor relative to conventional bulk thermoelectrics, however, it will be necessary to achieve cross-plane thermal conductivities in nitride superlattices that are of the order of 1 W/m K or lower while maintaining lattice coherency across the metal/semiconductor interface. Of several possible combinations of nitride metals and semiconductors,<sup>11</sup> ZrN and ScN have been selected for this study. ZrN is a metallic phase with the rocksalt structure, a bulk electrical resistivity of  $\rho=24$   $\mu\Omega$  cm (for stoichiometric ZrN) and a melting point of 2980 °C.<sup>13,14</sup> ScN is a rocksalt-structured semiconductor with a direct transition at the  $X$  point of 2.1 eV, a possible indirect transition from  $\Gamma \rightarrow X$  corresponding to an indirect bandgap in the range of 0.9–1.6 eV, and a melting point of  $\sim 2600$  °C.<sup>15–19</sup>

Most crystalline bulk and thin-film nitrides have thermal conductivities much greater than 1 W/m K. For example, the thermal conductivities measured in the present study for films of ZrN and ScN are  $\kappa=47$  and 10.6 W/m K, respectively. When grown in the form of metal/semiconductor superlattices with high interface densities, however, a substan-

<sup>a)</sup>Electronic mail: vrawat@purdue.edu.

<sup>b)</sup>Electronic mail: ykoh@mrl.uiuc.edu.

<sup>c)</sup>Electronic mail: d-cahill@uiuc.edu.

<sup>d)</sup>Electronic mail: tsands@purdue.edu.

tial reduction in thermal conductivity is anticipated. Furthermore, alloying the ZrN layers with  $WN_x$  to form (Zr,W)N/ScN metal/semiconductor superlattices was expected to reduce the thermal conductivity further while allowing the possibility of lattice matching.

## II. EXPERIMENTAL DETAILS

ZrN/ScN and (Zr,W)N/ScN multilayers and superlattices were grown on (100)MgO substrates using reactive dc magnetron sputtering in a load-locked turbomolecular pumped high vacuum deposition system with a base pressure of  $10^{-9}$  torr (PVD Products, Inc.). The growth chamber had the capability to hold four targets and was equipped with three dc power supplies. The targets for ZrN,  $W_2N$ , and ScN deposition were 2 in. diameter and 0.25 in. thick disks of Zr (99.7% purity), W (99.99%), and Sc (99.99%). All depositions were performed in Ar/ $N_2$  ambients with the flow rates of Ar and  $N_2$  and the total gas pressure inside the system maintained at 6 SCCM (SCCM denotes cubic centimeter per minute at STP), 4 SCCM, and 5 mtorr, respectively. The targets were sputtered in a constant power mode and the dc power was varied in the range of 10–200 W for a particular sample, depending on the desired stoichiometry and growth rates. The substrate was maintained at a temperature in the range of 830–1000 °C during deposition, as determined using an infrared pyrometer being operated at the spectral wavelength in the range of 0.8–1.1  $\mu\text{m}$ . In order to accurately determine the temperature of the MgO substrate, which is optically transparent in this wavelength range, a thin film of ZrN was deposited on the substrate and the temperature of ZrN film was measured. Due to the lack of available emissivity data for ZrN, we assumed the emissivity values to be in the range of 0.12–0.25 based on the optical reflectivity of similar sputter deposited ZrN films reported in literature.<sup>20–22</sup> Similar transition metal nitrides such as TiN and TaN also exhibit emissivities in this range. To ensure uniform film deposition, the substrate was rotated during the deposition.

Prior to deposition, the MgO substrates were ultrasonically cleaned in trichloroethylene, acetone, and isopropanol and then rinsed with de-ionized water, followed by blow drying in nitrogen. The substrates were annealed inside the deposition chamber at a temperature of 1000 °C for 30 min as this annealing step has been reported to show sharp MgO(001) ( $1 \times 1$ ) reflection high-energy electron diffraction (RHEED) reflections, which is desired for epitaxial film growth.<sup>23</sup> A 180 nm thick ZrN buffer layer was grown prior to the growth of the multilayer structure in order to accommodate an appreciable fraction of the lattice strain introduced by the 8% lattice mismatch between the MgO substrate ( $a=0.424$  nm) and the ZrN ( $a=0.458$  nm) layer. For one set of samples, in order to minimize the contribution of metallic ZrN to the electrical characteristics of the ZrN/ScN multilayers, the ZrN buffer layer was kept as thin as 10 nm.

Texture evolution and orientation relationships in the multilayers and superlattices were studied by x-ray diffraction using  $Cu K\alpha_1$  radiation in a Panalytical X'pert diffractometer equipped with triple-bounce monochromators to re-

move any contribution from  $Cu K\alpha_2$ . The period thickness of the superlattices was determined from the spacing between satellite peaks in x-ray diffraction patterns. Field emission scanning electron microscope (FESEM) imaging was used to determine the period thickness of multilayers that did not show satellite peaks in x-ray diffraction scans. Composition analysis of the multilayer films was performed using Rutherford backscattered spectrometry (RBS) using 2 MeV He<sup>+</sup> ions. The RBS spectra were fitted using an ion beam analysis simulation program (SIMNRA) to determine the composition of the samples.

The thermal conductivity of the multilayers was measured using the time-domain thermoreflectance (TDTR) technique.<sup>24,25</sup> Details of our setup are described in a previous publication.<sup>26</sup> In TDTR measurements, a train of short pulses (<0.5 ps) of a mode-locked Ti:sapphire laser is split into a pump beam and a probe beam. The pump beam is used to heat the samples and the temperature decay at the sample surface is monitored using thermoreflectance of the probe beam. The pump beam is modulated with an electro-optic modulator at a modulation frequency of 10 MHz, and changes in the intensity of the reflected probe beam at the modulation frequency were measured using a Si photodetector and a rf lock-in amplifier. The  $1/e^2$  radii of the pump and probe beam at the sample surface were fixed at 15  $\mu\text{m}$  and total laser powers of less than 35 mW were used to create temperature rises of less than 3 K. Prior to the measurement, the samples were coated with approximately 100 nm thick Al films, which were deposited by magnetron sputtering. The thermal conductivity of the multilayers was derived from fits of the calculations of a thermal model<sup>27</sup> to the measurements, taking into account changes in the radius of the pump beam at different relative delay times between the pump and probe pulses.<sup>28</sup>

## III. RESULTS AND DISCUSSION

Cross-sectional FESEM images of the ZrN/ScN multilayer samples confirmed the expected layered structure [Fig. 1(a)]. Symmetric  $\Omega-2\theta$  x-ray diffraction patterns (not shown) revealed only the 200 reflections from ScN and ZrN, whereas asymmetric  $\phi$  scans did not reveal distinct reflections. These data, along with FESEM imaging of fracture surfaces that revealed a columnar microstructure, indicate that the ZrN/ScN multilayers possess a uniaxial texture that is consistent with the local epitaxy of ZrN and ScN within the columnar  $\langle 100 \rangle$ -oriented grains. The addition of W–N to the ZrN layers significantly improved the structural quality of the multilayers, yielding epitaxial superlattices exhibiting superlattice reflections in the  $\Omega-2\theta$  x-ray patterns, as well as in-plane alignment as revealed by  $\phi$  scans. High-resolution  $\Omega-2\theta$  scans of  $Zr_{0.79}W_{0.21}N/ScN$  superlattices with periods ranging from 2 to 16 nm are shown in Fig. 1(b). Note that superlattice reflections are apparent for all periods in this range. Electron microscopy studies of these alloyed superlattices are reported in a separate publication.<sup>29</sup>

The dependence of the cross-plane thermal conductivity of ZrN/ScN multilayers on the multilayer period (or interface density) was studied using the TDTR technique. For this

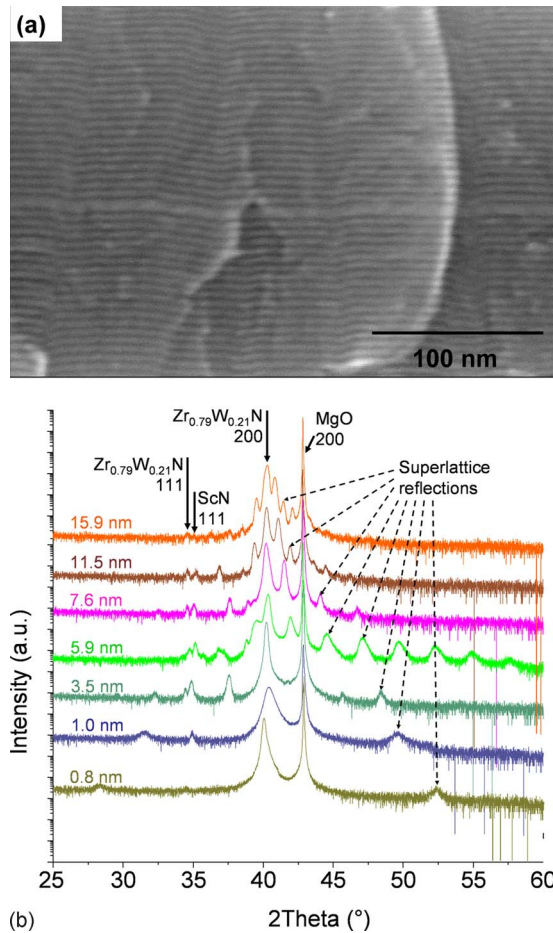


FIG. 1. (Color online) (a) Field emission scanning electron microscope image of the fractured cross-section of a ZrN(3 nm)/ScN(3 nm) multilayer. (b) High resolution x-ray diffraction scans obtained from a series of Zr<sub>0.79</sub>W<sub>0.21</sub>N/ScN superlattices with varying periods. The period values, obtained from the satellite reflections in x-ray diffraction patterns, are listed beside the diffraction patterns.

measurement, a set of ZrN/ScN multilayer samples was grown where the multilayer period, which is the sum of metal and semiconductor layer thicknesses, was varied while the thicknesses of the metal (i.e., ZrN) and the semiconductor (i.e., ScN) layers were kept equal. Figure 2 shows the total cross-plane thermal conductivity of ZrN/ScN multilayers (black circles) as a function of the multilayer period. Superimposed on the same plot is a dashed line corresponding to the room-temperature lattice thermal conductivity of a Zr<sub>0.65</sub>Sc<sub>0.35</sub>N alloy film of 300 nm thickness grown using simultaneous dc magnetron sputtering of Zr and Sc targets in a nitrogen ambient. In order to determine the lattice thermal conductivity of the Zr<sub>0.65</sub>Sc<sub>0.35</sub>N alloy film, first, the total thermal conductivity of the alloy film was measured using the TDTR technique and found to be 15.6 W/m K. The sheet resistivity of the Zr<sub>0.65</sub>Sc<sub>0.35</sub>N alloy film was then measured using a four point probe measurement to be 69.4 μΩ cm. The Wiedemann–Franz law was then used to calculate the electronic contribution to the thermal conductivity to be 10.6 W/m K, assuming a constant Lorenz factor of  $L=2.44 \times 10^{-8}$  W Ω K<sup>-2</sup>. The lattice contribution to the thermal conductivity was determined to be 5 W/m K after subtracting the electronic contribution from the total thermal

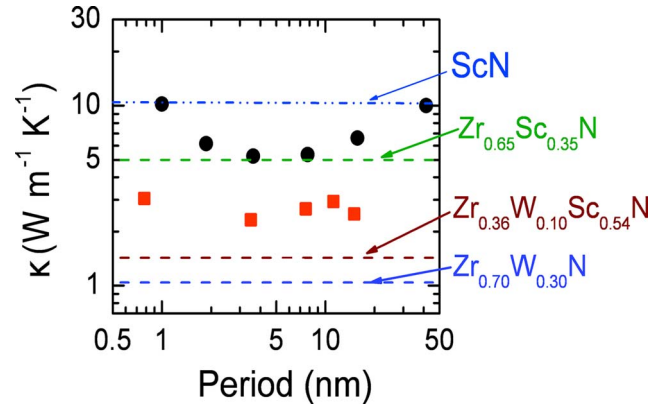


FIG. 2. (Color online) Cross-plane thermal conductivity of 300 nm thick ZrN/ScN (dots) and Zr<sub>0.64</sub>W<sub>0.36</sub>N/ScN (squares) multilayers. Superimposed on the plot are horizontal lines corresponding to the experimentally determined lattice component of thermal conductivity (i.e., alloy limit) of different alloys of ZrN, ScN, and W<sub>2</sub>N, namely, Zr<sub>0.65</sub>Sc<sub>0.35</sub>N, Zr<sub>0.36</sub>W<sub>0.10</sub>Sc<sub>0.54</sub>N, and Zr<sub>0.70</sub>W<sub>0.30</sub>N. The data points have an error bar that is equivalent to the size of the markers used to represent the measurement result.

conductivity, assuming thermal and electrical conductivities in the alloy film to be isotropic. This assumption regarding isotropic behavior is believed to be reasonable since the in-plane grain diameters were in the range of 150–250 nm as observed in cross-sectional FESEM images of the films, and this is comparable to the thickness of the films (~300 nm) that were used for the cross-plane thermal conductivity measurement. The lattice component of thermal conductivity was used as an estimate of the alloy limit for the ZrN/ScN materials system. The same process was used to estimate the lattice contribution of all control samples used in this study, and the results are summarized in Table I. Picosecond acoustics of the sample were analyzed to measure the longitudinal speed of sound along the cross-plane direction of thin-film control samples and those results were then used to estimate the elastic modulus  $C_{11}$ .<sup>30</sup> The longitudinal speed of sound and the elastic modulus ( $C_{11}$ ) are listed in Table II. The measured longitudinal speed of sound is similar to that of other metal nitrides such as TiN ( $v_1=10\,300$  m/s) (Ref. 31) and AlN ( $v_1=10\,127$  m/s).<sup>32</sup>

In Fig. 2, it can be seen that for a period larger than 6 nm, the thermal conductivity of the multilayers decreased monotonically with increasing interface density. For this range of period thickness, the thermal conductivity behavior is interface-controlled and in this regime, a lumped series resistance model treating the metal, the semiconductor, and the interface between them as three thermal resistors in series, can be used to describe the total cross-plane thermal conductivity. The cross-plane thermal resistance of the multilayer can be written as

$$\frac{d_{ML}}{\kappa_{ML}} = \frac{d_M}{\kappa_M} + \frac{d_S}{\kappa_S} + \frac{2}{G_{int}}, \quad (1)$$

where  $\kappa_{ML}$ ,  $\kappa_M$ , and  $\kappa_S$  are the total thermal conductivities of the multilayer, the metal layer alone, and the semiconductor layer alone, while  $d_{ML}$ ,  $d_M$ ,  $d_S$ , and  $G_{int}$  are the period of the multilayer, the metal layer thickness, the semiconductor layer thickness, and the thermal conductance (unit: W/m<sup>2</sup> K) of

TABLE I. Film composition, thicknesses, measured in-plane electrical resistivity, measured cross-plane thermal conductivity, and calculated lattice contributions to thermal conductivity using the Weidemann–Franz law for (Zr,W,Sc)N control samples analyzed in this work.

Film composition	Film thickness (nm)	In-plane electrical resistivity ( $\mu\Omega$ cm)	Measured cross-plane thermal conductivity (W/m K)	Estimated lattice contribution to thermal conductivity (W/m K)
ScN	306	...	10.6	10.6
ZrN	1450	26.7	47	19.5
Zr <sub>0.65</sub> Sc <sub>0.35</sub> N	297	69.4	15.6	5
Zr <sub>0.70</sub> W <sub>0.30</sub> N	600	271	3.75	1.04
Zr <sub>0.36</sub> W <sub>0.10</sub> Sc <sub>0.54</sub> N	600	1093	2.1	1.43

the interface, respectively. Thus, if the metal and semiconductor layer thicknesses are kept equal, then, from the slope of the total thermal conductivity versus period thickness, the interface thermal conductance ( $G_{\text{int}}$ ) can be estimated. From the slope of thermal conductivity versus period for periods greater than 6 nm (three samples), and using measured thermal conductivity values of 47 and 10.6 W/m K for ZrN and ScN, respectively, the interface conductance of ZrN/ScN multilayers is estimated to be about 200 MW/m<sup>2</sup> K, which is within the range of the interface conductances reported for intimate metal/nonmetal interfaces.<sup>33,34</sup>

It can also be seen in Fig. 2 that for periods smaller than 6 nm, the thermal conductivity increases with decreasing period, and a minimum in thermal conductivity of  $k = 5.25$  W/m K is observed for the multilayers with a period thickness of 6 nm. This value of thermal conductivity is much lower than the lattice contributions to the thermal conductivities of ZrN (19.5 W/m K) and ScN films (10.6 W/m K), but slightly higher than the alloy limit as estimated by the lattice component of a Zr<sub>0.65</sub>Sc<sub>0.35</sub>N film ( $k = 5$  W/m K). Similar thermal conductivity behavior has been reported in other materials systems such as Bi<sub>2</sub>Te<sub>3</sub>/Sb<sub>2</sub>Te<sub>3</sub> superlattices, where a thermal conductivity minimum was observed for a period of  $\sim 4$ –6 nm,<sup>8</sup> and GaAs/AlAs superlattices where a thermal conductivity minimum was observed for a period of  $\sim 2.2$  nm.<sup>35</sup> In the case of Bi<sub>2</sub>Te<sub>3</sub>/Sb<sub>2</sub>Te<sub>3</sub> superlattices, a minimum thermal conductivity that was about a factor of 2 lower than the alloy limit was obtained, while in the case of Si/Si<sub>0.7</sub>Ge<sub>0.3</sub> superlattices, the minimum thermal conductivity value approached the alloy limit.<sup>5</sup> A theoretical explanation for the minimum in cross-plane thermal conductivity of multilayers when the multilayer period becomes comparable to the mean free path of the dominant heat-carrying phonons has been described by Simkin and Mahan.<sup>36</sup> According to Simkin and Mahan,

under the assumption that superlattices have abrupt interfaces and minimal interface roughness, the phonons can be treated as particles only when the phonon mean free path is much smaller than the multilayer period. When the multilayer period becomes comparable to or smaller than the phonon mean free path, the phonons should be treated as waves; in this regime, phonon band folding effects become dominant over the phonon wave scattering at the interfaces leading to an increase in thermal conductivity with a decrease in multilayer period. We note that consensus is still not reached on whether phonon minibands facilitate heat transport in superlattices with ultrathin periods. In fact, recent studies on AlN/GaN superlattices with high quality interfaces indicate that heat transport of short-period superlattices is dominated by long-wavelength acoustic phonons, which are more weakly scattered by interfaces.<sup>37</sup>

For metal-semiconductor superlattices with ultrathin periods, there is an additional possibility for increase in thermal conductivity due to the increase in the electronic component of thermal conductivity at smaller periods. To test this hypothesis, temperature dependent measurements were performed on a ZrN(0.5 nm)/ScN(0.5 nm) multilayer (Fig. 3). This particular sample has a room temperature thermal conductivity approaching that of a ZrScN alloy. The temperature dependent thermal conductivity measurement performed on this sample showed that the thermal conductivity increases sharply with the increase in temperature. This rise in cross-

TABLE II. The longitudinal speed of sound and the elastic constant ( $C_{11}$ ) of control samples studied in this work.

Film composition	Longitudinal speed of sound, $v$ (m/s)	Elastic constant, $C_{11}$ (GPa)
ZrN	9600	672
ScN	7930	270
Zr <sub>0.70</sub> W <sub>0.30</sub> N	7270	494
Zr <sub>0.36</sub> W <sub>0.10</sub> Sc <sub>0.54</sub> N	7060	313

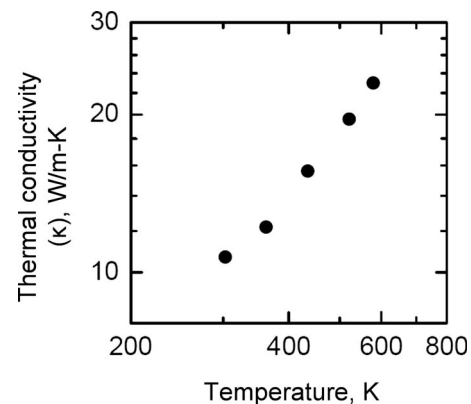


FIG. 3. Temperature dependent cross-plane thermal conductivity of 300 nm thick ZrN (0.5 nm)/ScN (0.5 nm) multilayer. The data points have an error bar that is equivalent to the size of the markers used to represent the measurement result.

plane thermal conductivity is similar to the rise in cross-plane electrical conductivity seen in such thermionic metamaterials,<sup>29</sup> thus, leading to the conclusion that for ultrathin period samples, the thermal conductivity is dominated by the electronic contribution.

At ultrathin periods, alloy scattering can be used to further suppress conduction of phonons with subnanometer wavelengths.<sup>38</sup> To this end, tungsten was investigated as an alloying element on the transition metal site in the metallic layer. Tungsten has a large atomic mass compared to Zr, and tungsten can form rocksalt-structured tungsten nitride, which can be alloyed with ZrN to yield a rocksalt (Zr,W)N alloy phase. Additionally, incorporation of tungsten substitutionally on zirconium sites in ZrN is expected to induce the formation of N vacancies, as the most stable composition of the W–N rocksalt phase has a nominal composition of  $W_2N$ . Furthermore,  $W_2N$  has a lattice parameter of 0.412 nm, smaller than that of both ZrN ( $a=0.458$  nm) and ScN ( $a=0.450$  nm). Thus, incorporation of about 14% W tungsten in Zr lattice sites should result in lattice-matched (Zr,W)N/ScN superlattices. Formation of such lattice-matched superlattices will promote the retention of a uniform layer structure for superlattice thicknesses of several tens of microns, as will be required for thermionic generator applications. In order to investigate the effect of tungsten alloying on the cross-plane thermal conductivity of  $Zr_xW_{1-x}N/ScN$  multilayers, a set of samples with W percentage of  $36 \pm 3\%$  with varying period thicknesses were grown. Figure 2 shows the effect of tungsten alloying on the cross-plane thermal conductivity of (Zr,W)N/ScN superlattices. The thermal conductivities of the W-alloyed samples are lower by a factor of 2 or more compared to the thermal conductivity of the corresponding ZrN/ScN superlattices. All the samples consistently show thermal conductivity values in the range of 2–4 W/m K, invariant of the period thickness, thus suggesting that in tungsten alloyed samples, alloy scattering is the dominant phonon scattering mechanism and not interface scattering. The alloy limit for the (Zr,W)N/ScN materials system was estimated by calculating the lattice component of the thermal conductivity of a  $Zr_{0.36}W_{0.10}Sc_{0.54}N$  film from the measured total thermal conductivity, yielding a value of 1.43 W/m K (Table I). It can be inferred from Fig. 2 that although there is a large reduction in thermal conductivity of the superlattices with tungsten alloying, the minimum achievable thermal conductivity value is still higher than the alloy limit. There is a small variation in period thicknesses due to the resputtering phenomenon, which is quite common in sputtered films and multilayers comprising of elements with very high back-scattering coefficient such as tungsten.<sup>39,40</sup>

In order to determine the amount of tungsten required to minimize the thermal conductivity in (Zr,W)N/ScN superlattices, a series of superlattice samples with a period of 6 nm was grown, in which the tungsten atomic percentage in the (Zr,W)N layer was varied in the range of 0%–100%. Figure 4 shows the cross-plane thermal conductivity variation as a function of tungsten atomic percentage on the transition metal site of the metallic nitride layer. It can be seen from the figure that substitution of 25% of Zr lattice sites in the ZrN layer with tungsten atoms can decrease the thermal conduc-

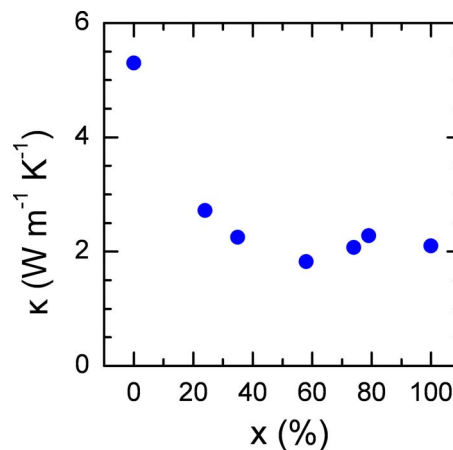


FIG. 4. (Color online) Cross-plane thermal conductivity of  $Zr_{1-x}W_xN$  ( $4.1 \pm 0.2$  nm)/ScN ( $2.0 \pm 0.2$  nm) superlattices as a function of tungsten content in the samples. The composition of the superlattices was measured using RBS.

tivity of the superlattice markedly. Further W additions had little effect, yielding a broad minimum with the lowest value of 1.8 W/m K recorded for a (Zr,W)N/ScN multilayer with 58% W on the transition metal site. Note that the epitaxial nature of the multilayers as indicated by the intensity of the 200 peaks of the (Zr,W)N and ScN layers in the x-ray diffraction patterns as well as the presence of superlattice reflections, was consistent for W percentage up to 35% in the metal layer and deteriorated for higher W percentages.

In summary, room temperature cross-plane thermal conductivity measurements of ZrN/ScN multilayers and (Zr,W)N/ScN superlattices are reported. A distinct minimum in thermal conductivity with superlattice period was seen in the ZrN/ScN multilayers, and the minimum thermal conductivity (5.25 W/m K) was comparable to the alloy limit (lattice component of the thermal conductivity of an alloy film). The upturn in thermal conductivity as the period is reduced below the value corresponding to the thermal conductivity minimum is likely due to the electronic contribution from carriers that are thermally excited over the metal/semiconductor barriers. Alloying the metal layers with tungsten leads to a significant reduction in thermal conductivity and the added effects of interface scattering, impurity scattering and/or acoustic impedance mismatch result in thermal conductivity values as low as 1.8 W/m K, a value that is a factor of approximately three lower than the mean value of 5.8 W/m K obtained from the measured values of 10.6 W/m K for a ScN film and the lattice component of 1.04 W/m K for a  $Zr_{0.70}W_{0.30}N$  film (Table I). The observation that room temperature thermal conductivities of metal/semiconductor nitride superlattices can be reduced to approximately 2 W/m K at compositions that allow matching of the ScN and (Zr,W)N lattice parameters bodes well for the future demonstration of high-performance metal/semiconductor solid-state thermionic generator materials.

## ACKNOWLEDGMENTS

This work was supported by ONR/DoD through a Multidisciplinary University Research Initiative (MURI) grant (program manager, Dr. Mihal Gross) and ONR Grant No.

N00014-07-1-0190. A portion of this work was carried out in the Center for Microanalysis of Materials, University of Illinois, which is partially supported by the U.S. Department of Energy under Grant No. DEFG02-91-ER45439.

- <sup>1</sup>G. D. Mahan and L. M. Woods, *Phys. Rev. Lett.* **80**, 4016 (1998).
- <sup>2</sup>A. Shakouri and J. E. Bowers, *Appl. Phys. Lett.* **71**, 1234 (1997).
- <sup>3</sup>J. M. O. Zide, D. Vashaee, G. Zeng, J. E. Bowers, A. Shakouri, and A. C. Gossard, *Phys. Rev. B* **74**, 205335 (2006).
- <sup>4</sup>D. Vashaee and A. Shakouri, *Phys. Rev. Lett.* **92**, 106103 (2004).
- <sup>5</sup>S. T. Huxtable, A. R. Abramson, C.-L. Tien, A. Majumdar, C. LaBounty, X. Fan, G. Zeng, J. E. Bowers, A. Shakouri, and E. T. Croke, *Appl. Phys. Lett.* **80**, 1737 (2002).
- <sup>6</sup>V. Narayanamurti, H. L. Störmer, M. A. Chin, A. C. Gossard, and W. Wiegmann, *Phys. Rev. Lett.* **43**, 2012 (1979).
- <sup>7</sup>S.-M. Lee, D. G. Cahill, and R. Venkatasubramanian, *Appl. Phys. Lett.* **70**, 2957 (1997).
- <sup>8</sup>R. Venkatasubramanian, *Phys. Rev. B* **61**, 3091 (2000).
- <sup>9</sup>G. Chen, *Phys. Rev. B* **57**, 14958 (1998).
- <sup>10</sup>A. Majumdar and P. Reddy, *Appl. Phys. Lett.* **84**, 4768 (2004).
- <sup>11</sup>V. Rawat and T. D. Sands, *J. Appl. Phys.* **100**, 064901 (2006).
- <sup>12</sup>D. Vashaee and A. Shakouri, *J. Appl. Phys.* **95**, 1233 (2004).
- <sup>13</sup>N. Farkas, G. Zhang, R. D. Ramsier, E. A. Evans, and J. A. Dagata, *J. Vac. Sci. Technol. A* **26**, 297 (2008).
- <sup>14</sup>H. O. Pierson, *Handbook of Refractory Carbides and Nitrides: Properties, Characteristics, Processing and Applications* (Noyes Publications, Westwood, NJ, 1996).
- <sup>15</sup>D. Gall, I. Petrov, N. Hellgren, L. Hultman, J. E. Sundgren, and J. E. Greene, *J. Appl. Phys.* **84**, 6034 (1998).
- <sup>16</sup>D. Gall, M. Stadelé, K. Järrendahl, I. Petrov, P. Desjardins, R. T. Haasch, T.-Y. Lee, and J. E. Greene, *Phys. Rev. B* **63**, 125119 (2001).
- <sup>17</sup>R. L. Lambrecht, *Phys. Rev. B* **62**, 13538 (2000).
- <sup>18</sup>C. Stampfl, W. Mannstadt, R. Asahi, and A. J. Freeman, *Phys. Rev. B* **63**, 155106 (2001).
- <sup>19</sup>A. R. Smith, H. A. H. AL-Britthen, D. C. Ingram, and D. Gall, *J. Appl. Phys.* **90**, 1809 (2001).
- <sup>20</sup>H. M. Benia, M. Guemmaz, G. Schmerber, A. Mosser, and J. C. Parlebas, *Appl. Surf. Sci.* **211**, 146 (2003).
- <sup>21</sup>S. Schlessner, T. Törndahl, and M. Edoff, *J. Phys.: Conf. Ser.* **100**, 082016 (2008).
- <sup>22</sup>M. Veszelei, K. Andersson, C. Ribbing, K. Järrendahl, and H. Arwin, *Appl. Opt.* **33**, 1993 (1994).
- <sup>23</sup>R. C. Powell, N.-E. Lee, Y.-W. Kim, and J. E. Greene, *J. Appl. Phys.* **73**, 189 (1993).
- <sup>24</sup>C. A. Paddock and G. L. Eesley, *J. Appl. Phys.* **60**, 285 (1986).
- <sup>25</sup>D. A. Young, C. Thomsen, H. T. Grahn, H. J. Maris, and J. Tauc, in *Phonon Scattering in Condensed Matter*, edited by A. C. Anderson and J. P. Wolfe (Springer, Berlin, 1986), p. 49.
- <sup>26</sup>D. G. Cahill, W. K. Ford, K. E. Goodson, G. D. Mahan, A. Majumdar, H. J. Maris, R. Merlin, and S. R. Phillpot, *J. Appl. Phys.* **93**, 793 (2003).
- <sup>27</sup>D. G. Cahill, *Rev. Sci. Instrum.* **75**, 5119 (2004).
- <sup>28</sup>Y. K. Koh and D. G. Cahill, *Phys. Rev. B* **76**, 075207 (2007).
- <sup>29</sup>M. Zabarjadi, Z. X. Bian, R. Singh, A. Shakouri, R. Wortman, V. Rawat, and T. Sands, *J. Electron. Mater.* (to be published).
- <sup>30</sup>T. Lee, K. Ohmori, C.-S. Shin, D. G. Cahill, I. Petrov, and J. E. Green, *Phys. Rev. B* **71**, 144106 (2005).
- <sup>31</sup>J. O. Kim, J. D. Achenbach, P. B. Mirkarimi, and S. A. Barnett, *Phys. Rev. B* **48**, 1726 (1993).
- <sup>32</sup>D. Gerlich, S. L. Dole, and G. A. Slack, *J. Phys. Chem. Solids* **47**, 437 (1986).
- <sup>33</sup>E. T. Swartz and R. O. Pohl, *Appl. Phys. Lett.* **51**, 2200 (1987).
- <sup>34</sup>R. J. Stoner and H. J. Maris, *Phys. Rev. B* **48**, 16373 (1993).
- <sup>35</sup>W. S. Capinski, H. J. Maris, T. Ruf, M. Cardona, K. Ploog, and D. S. Katzer, *Phys. Rev. B* **59**, 8105 (1999).
- <sup>36</sup>M. V. Simkin and G. D. Mahan, *Phys. Rev. Lett.* **84**, 927 (2000).
- <sup>37</sup>Y. K. Koh, Y. Cao, D. G. Cahill, and D. Jena, *Adv. Funct. Mater.* (to be published).
- <sup>38</sup>W. Kim, R. Wang, and A. Majumdar, *Nanotoday* **2**, 40 (2007).
- <sup>39</sup>D. B. Bergstrom, F. Tian, I. Petrov, J. Moser, and J. E. Greene, *Appl. Phys. Lett.* **67**, 3102 (1995).
- <sup>40</sup>M. M. Hasan, R. J. Highmore, and R. E. Somekh, *Vacuum* **43**, 55 (1992).